PHILOSOPHICAL TRANSACTIONS OF THE ROYAL SOCIETY A

Phil. Trans. R. Soc. A (2012) **370**, 2848–2865
doi:10.1098/rsta.2011.0378

Tubular precipitation structures: materials synthesis under non-equilibrium conditions

By Rabih Makki, László Roszol, Jason J. Pagano† and Oliver Steinbock*

Department of Chemistry and Biochemistry, Florida State University, Tallahassee, FL 32306-4390, USA

Inorganic precipitation reactions are known to self-organize a variety of macroscopic structures, including hollow tubes. We discuss recent advances in this field with an emphasis on experiments similar to 'silica gardens'. These reactions involve metal salts and sodium silicate solution. Reactions triggered from reagent-loaded microbeads can produce tubes with inner radii of down to 3 μm. Distinct wall morphologies are reported. For pump-driven injection, three qualitatively different growth regimes exist. In one of these regimes, tubes assemble around a buoyant jet of reactant solution, which allows the quantitative prediction of the tube radius. Additional topics include relaxation oscillations and the templating of tube growth with pinned gas bubble and mechanical devices. The tube materials and their nano-to-micro architectures are discussed for the cases of silica/$Cu(OH)_2$ and silica/$Zn(OH)_2$/ZnO tubes. The latter case shows photocatalytic activity and photoluminescence.

Keywords: self-organization; precipitation reactions; silica

1. Introduction

Modern materials science has evolved into a highly cross-disciplinary research field spanning physics, chemistry, biology and engineering. This ongoing fusion of traditional disciplines creates tremendous opportunities and will yield synthetic strategies that differ radically from today's standard approaches [1,2]. It is not too adventurous to predict that many of these approaches will imitate or at least be reminiscent of biological processes [3,4]. A good example for this prediction is current research on self-healing materials which aims to introduce a typical feature of living matter—the ability to regenerate after damage or injury—into man-made polymer and hybrid materials [5–7]. Another example is the creation of self-propelled micro- and nanoparticles capable of transporting cargo over macroscopic distances [8–12]. Important ingredients of these efforts include non-equilibrium conditions, compartmentalization and reaction–transport coupling [13–19].

*Author for correspondence (steinbck@chem.fsu.edu).
†Present address: Department of Chemistry, Saginaw Valley State University, University Center, MI 48710-0001, USA.

One contribution of 14 to a Theme Issue 'Beyond crystals: the dialectic of materials and information'.

Figure 1. Tubular precipitation structures formed by seeding small particles of $FeCl_3$ and $CoCl_2$ into a 1.5 M solution of sodium silicate. Scale bar: 5 mm. (Online version in colour.)

The latter features are all combined in silica (chemical or crystal) gardens that belong to one of chemistry's oldest experimental systems [20–23]. In its classic form, this experiment is frequently used as a demonstration experiment and chemical toy because it forms colourful, hollow structures that grow and move in a life-like fashion [24,25] (figure 1). It is hence no surprise that this system has attracted the interest of generations of scientists and laypeople, including Isaac Newton, Johann Rudolf Glauber, Stephane Leduc, Thomas Mann and Oliver Sacks [26–31]. The self-organizing process is started by placing a 'seed' particle into aqueous solutions containing anions such as silicate, borate, phosphate or carbonate. Apparently, all metal salts can serve as seeds with the exception of group 1A compounds. In solution, the salt dissolves and releases metal ions into the alkaline solution where they precipitate a thin colloidal membrane of compounds such as metal hydroxides, metal oxides and metallo-silicates. The membrane encapsulates the seed particle and stretches owing to the osmotically driven inflow of water. Once it bursts, a buoyant jet of salt solution is ejected and templates the growth of complicated precipitation structures such as nodules and tubes. The tubes have diameters of typically 0.1–1 mm and can reach lengths of several centimetres.

In the early 1990s, several groups recognized the potential of the silica-garden system for materials science. Collins *et al.* [32,33] reported that tube walls consisting of alumino-silicates are powerful Brønsted catalysts. Klinowski and co-workers [34] also discovered a complex hierarchical architecture in the same material that extends from the molecular level to micrometre-sized domains and finally to the macroscopic tube shape. Moreover, Balköse *et al.* [35] characterized various tube structures using analytical techniques, including infrared spectroscopy and X-ray diffraction measurements. They also reported Brunauer–Emmett–Teller and Langmuir surface area data from N_2 and H_2O adsorption, which were in the range of 10–300 $m^2\,g^{-1}$, and total pore volumes

around $0.15\,cm^3\,g^{-1}$. In addition, the physico-chemical description of the growth process has attracted renewed interest as exemplified by the study of Cartwright *et al.* [36], who studied concentration changes in the solution surrounding the tubes using Mach–Zehnder interferometry.

The first microgravity study on silica gardens was carried out by Jones & Walter [37,38]. Their experiments produced samples that were qualitatively similar to precipitation structures formed on the Earth. This result established unambiguously that precipitation tubes do not require gravitational convection. More recently, Cartwright *et al.* [39] published results obtained at the International Space Station. These experiments employed seed particles of calcium, manganese and cobalt chloride as well as nickel sulphate. The study shows that tube growth under microgravity conditions is much slower than on the Earth. A direct consequence of this difference is the existence of plastic deformations induced by the swelling of the precipitation membrane. Cartwright *et al.* also observed undulating tubes that might be caused by a diffusion-limited growth regime relevant only in the absence of gravity-driven flows.

Other recent advances include work by Cronin and co-workers [40,41], who demonstrated the formation of microtubes from polyoxometalate-based crystals in solutions containing dihydroimidazophenanthridinium (DIP) cation. The growth direction and the outer radius of these structures can be affected by externally applied electric fields as well as transient gradients in DIP concentration [42]. Pantaleone *et al.* [43,44] reported rhythmic motion of tubes in a $Ca(NO_3)_2$/silicate system. During these relaxation oscillations, tube segments bend downward and suddenly 'twitch' upwards. Theoretical analyses of the stresses in the pre-wall membrane reveal that the 'young' membrane is 5–10 times weaker than the well-established precipitation membrane. The simultaneous pressure oscillations have average amplitudes of 20–300 Pa [44].

Another line of research on precipitation tubes focuses on hydrothermal vents and has been pursued by Russell and co-workers [45,46]. Their primary interest is the possible role of these structures in prebiotic chemistry. Large under-sea vents such as 'lost city' contain magnetite, brucite ($Mg(OH)_2$) and serpentine which is a hydroxylated magnesium–iron silicate. The wall structures are exposed to tremendous concentration, pH and temperature gradients. These gradients in conjunction with catalytic surfaces are likely to sustain complex chemical reactions. The question whether this complexity matches the necessary conditions for prebiotic chemistry is obviously still unanswered.

Out of this rich research spectrum, we will focus on the description of laboratory-scale silica-garden systems that use quantifiable means of reagent delivery. This study will also present novel results on the morphology of microstructures and review recent progress towards a full quantitative control and understanding of these systems.

2. Microtubes

What is the lower limit for the radius of silica-garden-derived precipitation tubes? The answer to this intriguing question is unknown. In 2009, Makki *et al.* reported the synthesis of tubes with an inner radius of 3 μm [8]. This value—which

currently is the smallest value on record—is about the same as the smallest blood capillaries in the body. It is also three orders of magnitude larger than the radius of molecular tubes, such as single-wall carbon nanotubes which have a typical diameter of close to 1 nm [47]. In the intermediate size range, we find hollow tubes produced by organic templating procedures. For instance, Nakamura & Matsui [48,49] reported the formation of hollow silica nanotubes with square-shaped cross sections in an ethanolic tetraethyl orthosilicate (TEOS) solution containing DL-tartaric acid and ammonium hydroxide. These tubes have inner diameters of 20–800 nm. They are believed to grow around crystals of ammonium DL-tartrate that form when ammonium hydroxide solution is added to TEOS/tartaric acid solution [50,51]. Considering the latter example, it seems likely that template-free submicrometre silica gardens can be produced. However, this question requires further attention, and its experimental and theoretical investigation might reveal interesting dependencies on diffusion coefficients, reaction rates as well as nucleation and aggregation processes.

The aforementioned work by Makki *et al.* [8] is based on a novel technique for the production of hollow silica tubes. As mentioned in §1, the conventional method involves the use of small grains of a particular metal salt. Maselko *et al.* [43] improved this method by using pressed pellets which provide better control and a higher reproducibility compared with random (often polycrystalline) seed particles. However, the production of very small pellets is challenging. For this reason, Makki *et al.* employed small polymer beads. These beads are produced by emulsification techniques and then loaded with one of the two reagents (i.e. silicate or metal ion) by simple equilibration in aqueous solution. Once exposed to the other reagent, the beads rapidly surround themselves with a colloidal membrane. In the course of the reaction, this membrane hardens which induces crack formation and immediate self-healing owing to a renewed, rapid precipitation. Scanning electron micrographs (SEMs) of the product structures show the self-healed cracks as elevated rims on otherwise smooth spherical capsules [8]. In addition to these processes, the reacting beads produce microtubes (figure 2*a*). For the sodium silicate/cupric sulphate system, tube formation is observed only above a critical bead radius; below this radius, the reaction forms a thin shell around the bead surface but not outward-extending structures or tubes. To a good approximation, the critical radius is inversely proportional to the initial loading concentration. This dependence is due to metal ion consumption during the initial formation of the spherical envelope and the resulting shell. Owing to the surface-to-volume ratio of spheres, this consumption is relatively large for small beads. Hence, small beads (with radii below the critical radius) deplete most of their reactant load for shell formation and subsequently fail to produce tubes.

Analyses of video-microscopy data from the latter experiments show that microtubes grow at speeds of 20–50 $\mu m\,s^{-1}$. Typically, the growth velocity is not constant but tends to decrease in a non-trivial fashion. The velocity changes correlate with changes in the micrometre-scale morphology of the tube wall. While fast tube growth gives rise to smooth tubes, slow tube growth induces brick-like morphologies. Three representative examples are shown in figure 2*b–d*. It is likely that the brick-like structures are caused by the nucleation of small crystallites (5–20 μm) that form only if the tube-extending reaction front proceeds slowly. Clearly, more data are needed to verify this hypothesis.

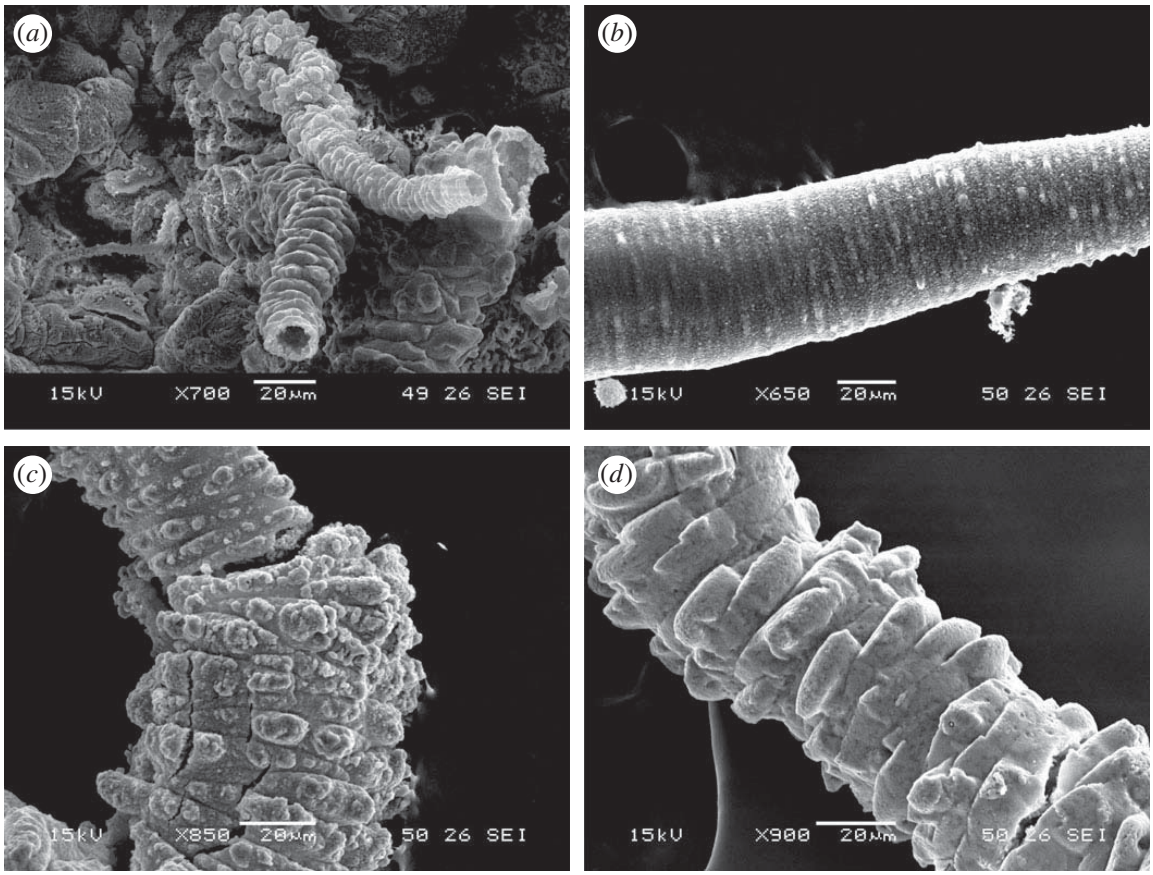

Figure 2. SEMs of precipitation tubes formed by compartmentalization of the two reactants, cupric sulphate and silicate, into small agarose beads and an outer solution reservoir, respectively. (*a*) A pair of tubes with inner radii of below 10 µm. (*b–d*) Three examples of the outer tube surfaces with textures ranging from smooth (*b*) to brick-like in (*d*). Scale bars: 20 µm.

3. Growth regimes under flow injection

All techniques discussed so far involve a finite reservoir of metal ions, namely crystalline or polycrystalline particles, pellets and reagent-loaded polymer beads. In 2003, Thouvenel-Romans & Steinbock [52] described a method in which the metal ions are delivered hydrodynamically by the injection of aqueous solution through a glass nozzle. This approach allows the study of tube formation under nearly constant reaction conditions. Typically, it employs constant pump rates Q and large reservoirs of silicate solution. Notice that under these conditions, all main system parameters are readily quantifiable. These include the temperatures, concentrations, pH values, viscosities and densities of the fluids in the reservoir and the injection stream as well as the selected pump rate. Because the parameters of the injected fluid can change during its motion from the injection point to the top of the growing tube, some transients still remain. Related phenomena, however, appear to be difficult to observe and should be relevant only for slow pump rates or very long tubes.

The aforementioned injection method allows the quantitative description of three distinct growth regimes [52]. In the following, we will refer to these dynamics as ‘jetting’, ‘popping’ and ‘budding’. At constant silicate concentration and

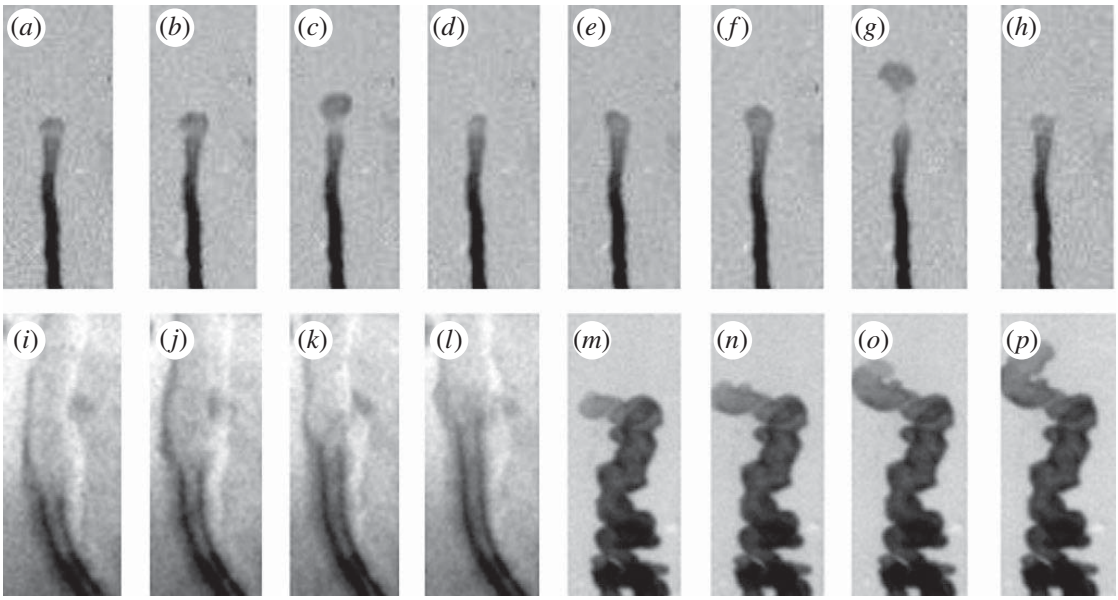

Figure 3. Image sequences illustrating popping growth (*a–h*), jetting growth (*i–l*) and budding growth (*m–p*). Pump rate: 7.0 ml h^{-1}. Silicate concentration: 1 M; cupric sulphate concentrations: 0.25 M (*a–h*), 0.05 M (*i–l*) and 0.50 M (*m–p*). Reprinted with permission from Thouvenel-Romans & Steinbock [52].

constant pump rate, these regimes depend critically on the density difference $\Delta\rho$ between the outer silicate solution and the injected reactant solution. For high values of $\Delta\rho$ (e.g. low concentration of the metal salt), tube growth proceeds steadily around a highly buoyant jet (figure 3*i–l*). Notice that in the figure, the tube appears darker than the fluid jet. At decreased buoyancy, this growth mode becomes unstable and gives rise to an oscillatory form of growth (figure 3*a–h*). It is likely that the onset of this instability is closely related to the strength of diffusive and convective fluxes in the growth zone. Typical periods and growth velocities are 0.5–15 s and 0.05–0.35 mm s^{-1}, respectively. In our experimental set-up, the injection is stopped when the tubes reach a length of 20–30 cm. The oscillations are relaxation oscillations and involve the periodic capping of the growth zone with a membranous envelope. This envelope expands under the inflow of fresh reactant solution and produces a fluid-filled balloon of increasing buoyant force. The rate of this expansion matches the employed pump rate. The mechanical contact between the balloon and the primary tube yields at a particular force; subsequently, the balloon pops off and floats towards the top of the silicate reservoir. At even lower buoyancy (figure 3*m–p*), the expanding balloon stays attached to the main structure but undergoes a local breach triggering the formation and subsequent growth of similar nodules. This regime is referred to as budding growth and has not been characterized yet.

For popping dynamics, the distribution of time intervals between subsequent detachment/breach events is much narrower than for budding growth. The average popping period T can be described semi-empirically by considering the buoyancy force of the membrane-bound envelope F which equals $g\Delta\rho V$, where g is the Earth's gravity and V denotes the envelope volume. The fluid

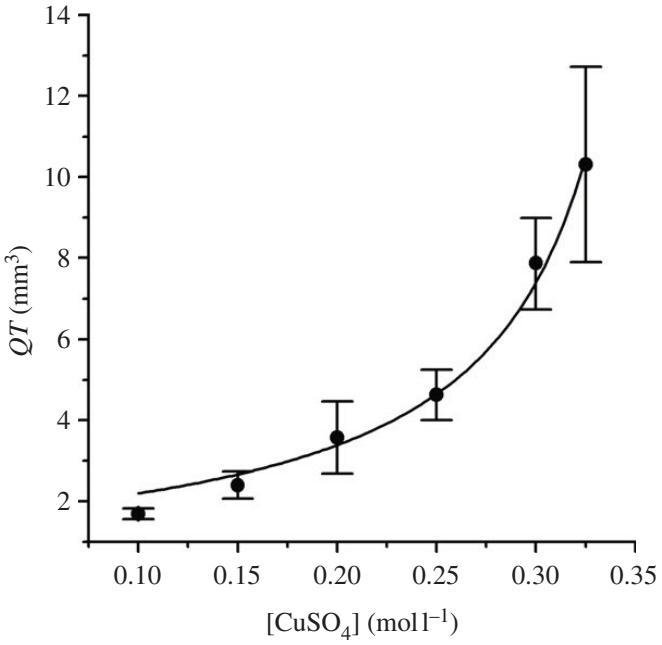

Figure 4. The volume of solution, QT, delivered during one period of the oscillatory popping dynamics increases with increasing concentrations of cupric sulphate. Each datum point is the average of several experiments at different flow rates in the range of 2–15 ml h^{-1}. The continuous line is a fit based on equation (3.2). Reprinted with permission from Thouvenel-Romans & Steinbock [52].

volume delivered per period, QT, yields a force F_{crit} sufficient to induce detachment. Hence,

$$F_{\mathrm{crit}} = g\Delta\rho QT. \tag{3.1}$$

To a very good approximation, we find that the density difference is a linear function of the metal salt concentration c obeying $\Delta\rho = \rho_{\mathrm{o}} - \rho_{\mathrm{w}} - \xi c$, where ρ_{o} and ρ_{w} are the density of the silicate solution and pure water, respectively, and ξ is the partial derivative of the density of the salt solution with respect to its concentration. We thus obtain

$$T = \frac{F_{\mathrm{crit}}}{gQ(\rho_{\mathrm{o}} - \rho_{\mathrm{w}} - \xi c)}. \tag{3.2}$$

This simple equation is in good agreement with experimental data. The example shown in figure 4 was obtained for the silicate/cupric sulphate system and yielded—by means of least-square fitting—a detachment force of $F_{\mathrm{crit}} = 2\,\mu\mathrm{N}$. From this force value, one can estimate the tensile strength of the relatively fresh tube material underneath the membrane envelope. The resulting values are very small which is expected for a soft, colloidal membrane. Lastly, we note that in the popping regime, vertical tube growth is surprisingly fast reaching average speeds v of 0.35 mm s^{-1}. Furthermore, it was reported that the average growth distance per period vT is widely independent of the flow rate Q [52]. However, vT increases for high metal salt concentrations.

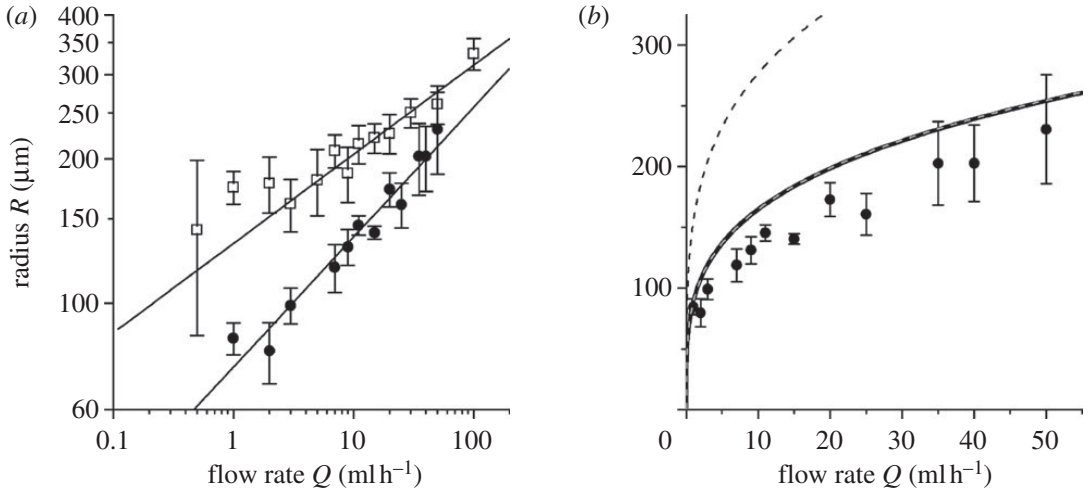

Figure 5. (*a*) Flow rate dependence of the outer radius of silica tubes. Solid circles and open squares indicate seed concentration of $[CuSO_4] = 0.075\,\mathrm{mol\,l^{-1}}$ (jetting growth) and $0.15\,\mathrm{mol\,l^{-1}}$ (popping growth), respectively. The jetting data are shown again in (*b*) along with the solutions of purely hydrodynamic equations. The solid curve and the nearly identical dashed line correspond to a model without adjustable parameters (cf. equations (4.1)) with the latter curve being the approximation specified in the text. The steeper dashed curve corresponds to the stiff tube model (i.e. equation (4.2) for $\eta_o \to \infty$). Reprinted with permission from Thouvenel-Romans *et al.* [53].

4. Radius selection in the jetting regime

Tube growth at low concentrations of the injected solution (high buoyancy) appears to be the dynamically simplest case of the aforementioned growth regimes. All qualitative observations of jetting growth suggest that the tube is templated around the buoyant jet of reactant solution. This hypothesis was tested by Thouvenel-Romans *et al.* [53]. That study measured the outer tube radius from optical micrographs. Figure 5 shows these data as a function of flow rate. In all measurements, the outer silicate solution was confined to a glass cylinder of radius $R_{cyl} = 1.1\,\mathrm{cm}$. The double-logarithmic plot in figure 5*a* shows that jetting and popping growth can be described by power laws with exponents of 0.27 ± 0.02 and 0.18 ± 0.02, respectively. Figure 5*b* shows the same jetting data along with a direct comparison with theoretical description of the radius.

This description focuses strictly on the fluid dynamics while neglecting reactions, diffusion and interfacial tension. The model further assumes negligible velocity differences and shear stress across the forming tube wall. The buoyant cupric sulphate solution ascends as a cylindrical jet of radius R. The cylindrically symmetric velocity fields $v(r)$, which solve the Navier–Stokes equations, are then

$$v_o = A_o \ln r + B_o + C_o r^2, \quad v_i = B_i + C_i r^2, \tag{4.1}$$

where the indices 'o' and 'i' denote the outer and inner fluid, respectively. Notice that there is no logarithmic term in the expression for v_i because the velocity in the jet cannot diverge.

All five constants in equations (4.1) are known if one considers the following appropriate boundary conditions: (i) stick boundary condition at the container wall $v_o(R_{cyl}) = 0$; (ii) continuity of velocity, shear stress and pressure at the fluid interface $r = R$; and (iii) a constraint of no-mean-flow for the outer fluid (the volume of the silicate solution is constant) [53]. Hence, for a given set of one radius (R), two viscosities ($\eta_{i,o}$) and two densities ($\rho_{i,o}$), both flow fields are fully determined. They yield the pump rate Q from $v_i(r)$ and hence a unique relation between Q and R. The corresponding equation ($Q(R)$) can be expressed in an algebraic form but is unfortunately very cumbersome. However, in the relevant limit $R_{cyl} \gg R$, it simplifies to

$$Q = \frac{\pi g(\rho_o - \rho_i)}{(8\eta_i)R^4\{1 + (4\eta_i/\eta_o)[\ln(R_{cyl}/R) - 1]\}}. \tag{4.2}$$

This equation is similar to the classic Hagen–Poiseuille law but includes a correction for the jet-driven motion in the outer liquid.

The direct comparison between the theory (equation (4.2); solid curve in figure 5*b*) and the experimental data yields excellent agreement. This finding confirms the initial hypothesis that jetting tube growth (i) is a templating process around a buoyant jet of reactant solution and (ii) creates precipitation structures with radii that are determined by the underlying hydrodynamics. Clearly, popping and budding growth do not allow a similar description. On the contrary, fluid dynamics do not play any relevant part in their dynamics. In addition, the vertical growth velocity of jetting tubes cannot be described in terms of a simple hydrodynamic model as it requires additional information on reaction rates and diffusion. To date, no quantitative or semi-quantitative model for any of the latter phenomena exists.

5. Radius selection with bubbles

One of the remarkable features of chemical gardens is that (highly buoyant) gas bubbles can pin to the growth zone of the forming tube. Once in place, the bubble is held in the growth region by interfacial tension and moves in an upward direction at a velocity that matches the speed of tube formation. This phenomenon was first reported for seed-grown structures by Hazlehurst [54] in 1941. It is a rather common phenomenon because when submerged into the silicate solution, seed particles tend to trap small air bubbles on their surface. Thouvenel-Romans *et al.* [55] noted that tubes with pinned bubbles form more quickly and are much straighter than their bubble-free counterparts. Their radius tends to decrease in upward direction; probably owing to the steady dissolution of the seed and a resulting decrease in osmotic pressure.

These observations are used to further improve the injection-controlled set-up [55]. For this purpose, a thin steel needle is introduced into the glass nozzle to deliver a small volume of gas into the flow of salt solution. The needle is connected to a syringe, which allows the control of the injection volume and, hence, the size of the gas bubble. With this modification, bubble-guided tubes are produced reliably under conditions of well-defined and measurable

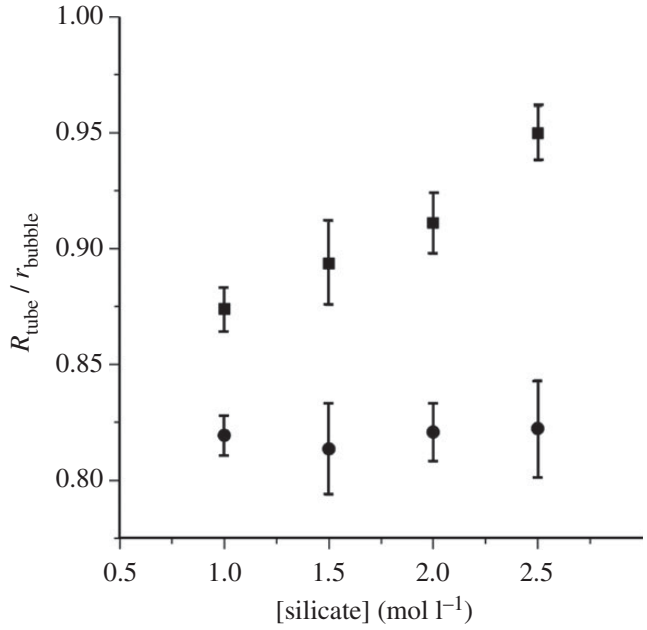

Figure 6. Average ratio between the outer tube radius and the radius of the templating bubble. Solid circles and squares correspond to flow rates of 3 and 10 ml h^{-1}, respectively. All experiments involve the injection of 0.5 M cupric sulphate solution.

physical and chemical parameters. As expected from the growth of bubble-capped, seed-grown structures, the resulting tubes are very straight and have a constant radius.

The latter study also established that tubes with pinned bubbles increase their (enclosed) volume at the rate of flow injection. This volume conservation implies that the speed v of tube growth in vertical direction is described by the simple equation

$$v = \frac{Q}{\pi R^2}, \tag{5.1}$$

where R denotes the tube radius. Notice that this equation also holds for popping growth during the phase of membrane-cap expansion. Furthermore, it is likely to be applicable to budding growth but no data are available. However, for open growth regimes such as jetting, equation (5.1) provides only a very generous upper limit for v.

For the parameter range studied by Thouvenel-Romans *et al.* [55], the tube radius R is similar to the bubble radius r. The results in figure 6 show that R/r varies systematically in the range of 0.8–0.95. The largest ratios are found for high flow rates and high silicate concentrations. In addition, we observe that the ratio is constant at low flow rates; at higher flow rates, however, the value increases with increasing silicate concentration. These findings are important because they establish that the gas bubble selects the tube radius. Consequently, this template-like function indirectly selects (at a given pump rate Q) a unique growth velocity v according to equation (5.1). The physical mechanisms behind these processes are unclear but one can speculate that the flow field around the bubble could play an important role.

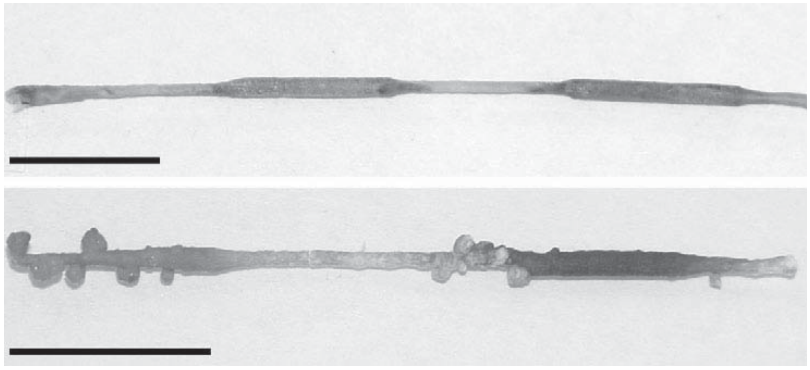

Figure 7. Tube growth under externally controlled oscillations of the linear growth velocity. The velocity is alternated between $v_s = 2$ and $v_f = 6\,\mathrm{mm\,s^{-1}}$. The low and high velocity values are maintained for 6 and 2 s, respectively, to achieve an equal travel distance of 12 mm. The pump rate is kept constant at $Q = 10\,\mathrm{ml\,h^{-1}}$. The wider (thinner) parts of the samples form at slow (fast) rod velocities. The original growth direction is left to right. Notice the nodules in (*b*). Scale bars: 1 cm.

6. Mechanical control of the growth velocity

The experiments described in §5 motivated a study by Makki *et al.* [56] in which the growth velocity v of the silica tube was controlled by pinning the growing tube to an upward moving rod. More specifically, this approach was demonstrated for the injection of cupric sulphate solution into sodium silicate solution. The forming tube was pinned to the end of a hollow glass rod with a large gas bubble (diameter of about 4 mm) serving as a non-sticky interface. The study established that the tube's vertical growth follows the speed of the glass rod (0.5–$11\,\mathrm{mm\,s^{-1}}$). Its radius, however, was found to self-select according to the volume of the injected solution (see equation (5.1)).

Another result of the study in Makki & Steinbock [56] is that tube growth can occur either at the moving gas bubble or at the stationary glass nozzle. Notice that in all earlier examples, the lengthening growth of the tube occurred strictly at the upper end of the tube (i.e. at the tube end farthest from the source of internal reactant). The novel 'bottom growth' occurs for large velocities, which might not be easily accessible without this specific set-up. The critical velocity v_{crit} between 'top' and 'bottom' growth obeys a power law of the form

$$v_{crit} = kQ^{1/2}. \tag{6.1}$$

The proportionality constant for the specific conditions in the study was reported as $k = 3.7\ (\mathrm{mm\,s})^{-1/2}$.

Perhaps the most interesting finding results from experiments in which the velocity of the pinning glass rod (and hence the velocity of tube growth) is periodically switched between a high and a low value [56]. During this forcing, the pump rate Q and all other parameters are kept constant. The tubes formed under such conditions have periodic variations in their outer radius. Two typical examples are shown in figure 7. The changes in the outer radius are in good quantitative agreement with equation (5.1). However, within the

transition regions, more complex dynamics can be observed. For a sudden increase in velocity, the radius decreases not abruptly but reveals a noticeable relaxation process. This smooth relaxation must depend on the visco-elastic and mechanical characteristics of the forming membrane but has not been analysed yet. More striking is the formation of numerous nodules during each sudden decrease in rod velocity (figure 7*b*). These nodules are hollow and found only on the outer tube surface. Their formation is closely related to the sudden pressure increase in the tube's interior and the inability of the tube to change its radius instantaneously. Nonetheless, nodules are observed occasionally also under static conditions and—in general—their occurrence is subject to fluctuations of unknown origins.

Statistical analyses show that under the experimental conditions of Makki's study, an average of $N_\infty = 10$–12 nodules forms per velocity drop. Their cumulative number $N(t)$ obeys

$$N(t) = N_\infty \left(1 - \exp\left(\frac{-t}{\tau}\right)\right), \tag{6.2}$$

where $t = 0$ represents time of the velocity change. The relaxation constant is $\tau = 2.6\,\mathrm{s}$. From the average volume V_b of the (nearly spherical) nodules, one can further reproduce the initial rate of nodule formation using

$$\frac{\mathrm{d}N}{\mathrm{d}t} = \frac{(v_\mathrm{f} - v_\mathrm{s})\,Q}{v_\mathrm{f}\,V_\mathrm{b}}, \tag{6.3}$$

where v_f and v_s denote the fast and slow rod velocity, respectively.

The asymmetry of the described nodule instability with respect to sign of the velocity jump has an interesting analogue in a non-reactive membrane system which we wish to mention briefly. The inflation of several connected and identical rubber balloons does not occur simultaneously but sequentially owing to a non-monotonic pressure–volume isotherm [57]. Deflating balloons, however, decrease their volume in synchrony.

7. Materials characterization

Qualitative as well as spectroscopic techniques can be used to characterize the tube material which we discussed so far mainly in terms of its macroscopic features. We will limit our discussion to experiments employing sodium silicate solution in the outer reservoir and metal sulphate solution (not group 1A) as the injection- or seed-delivered fluid. Under these conditions, the tube wall typically shows a strong radial composition gradient. The exterior layers are rich in silica and the interior layers are rich in metal hydroxide [58]. This feature is illustrated in figure 8 for the example of tubes formed under cupric sulphate injection. Figure 8*a*,*b* shows SEM–energy dispersive X-ray spectroscopy (SEM-EDS) data for the outer and inner tube surface, respectively. Notice the difference in the Cu-to-Si ratio between the data obtained for the outer (figure 8*a*) and the inner surface (figure 8*b*). Figure 8*c* shows a cross section of the tube wall revealing two distinct layers and complex (possibly crystalline) structures on the inside surface. The bottom portion of figure 8*c* shows a schematic that relates the tube wall morphology as seen in SEM to the likely concentration profiles during

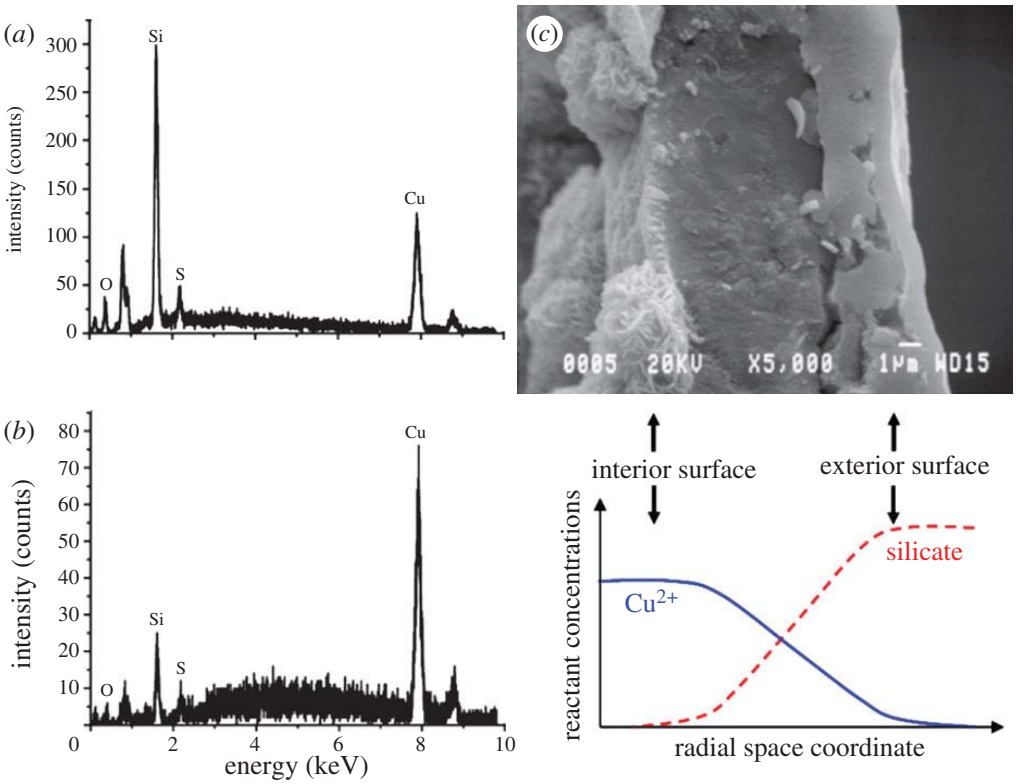

Figure 8. EDS spectra of the exterior (*a*) and interior surface (*b*) of a typical precipitation tube. (*c*) SEM micrograph of a small wall segment. The exterior and interior surfaces extend along the right and left image border as indicated by the arrows. The schematic shows the likely concentration profiles of the reactant species (Cu^{2+} and silicate ions) across the forming tube wall. (Online version in colour.)

tube formation. While this picture provides a very qualitative explanation of the observed compositional gradients, it will clearly require more detailed theoretical efforts to obtain a satisfying description.

The thickness of the wall in figure 8 is approximately 10 µm. This value seems to be characteristic for injection-controlled tube formation under a wide range of experimental parameters. Notice however that the microtubes formed from reagent-loaded gel beads (figure 2) have a thickness in the range of 1–5 µm. The mechanism that controls the wall thickness is not understood yet. One can speculate that transport processes must play a key role. Moreover, the steep pH gradient across the reaction zone and the self-termination (or at least self-inhibition) of the precipitation reaction by compartmentalization are important factors. Roszol & Steinbock [59] studied the increase in wall thickness under conditions of sustained reagent delivery. Their results show that radial wall growth occurs only in an inward direction. Furthermore, the wall thickness can increase with time according to simple square root functions which directly suggests a diffusion-controlled mechanism.

In 2008, Pagano *et al.* [60] reported the production of very straight, high-aspect ratio silica tubes in the reaction between $ZnSO_4$ and sodium silicate. Their preparation employs the flow injection and free-bubble templating discussed earlier in this study. After completion of the tube synthesis, the hollow samples

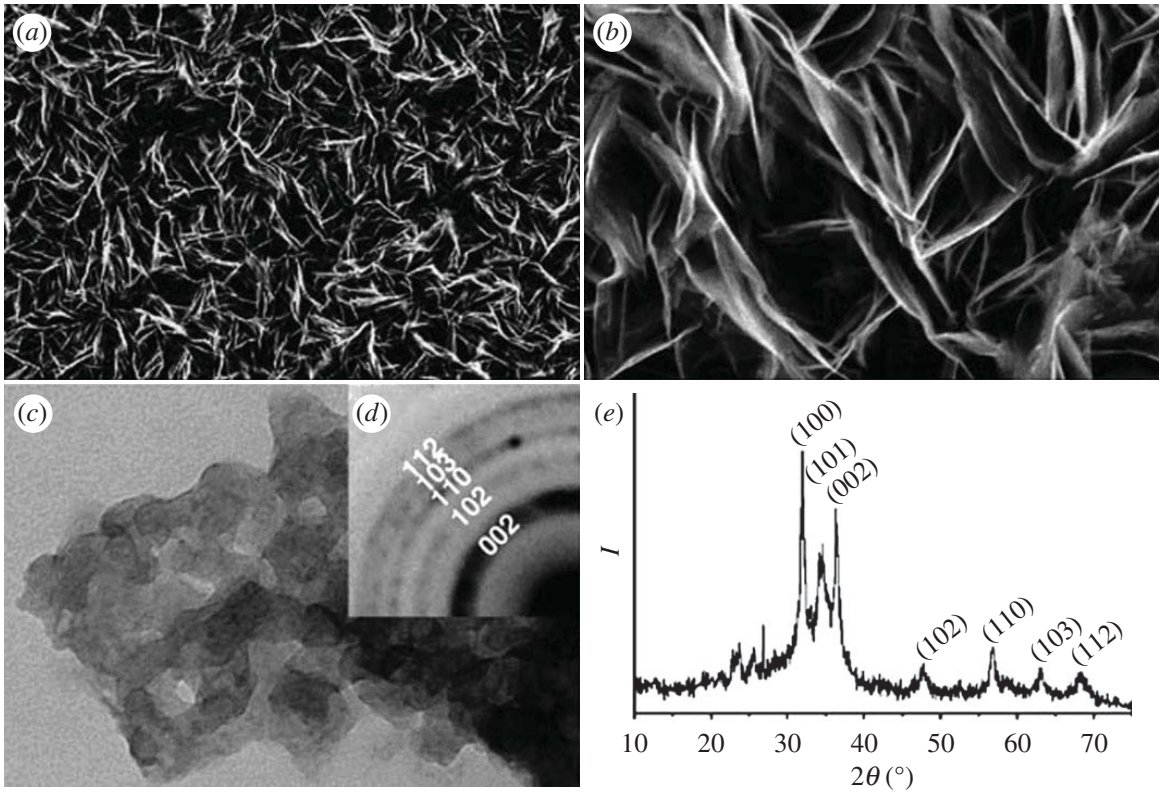

Figure 9. Tubes formed under bubble guidance and flow injection of $ZnSO_4$ solution into sodium silicate solution. After heating to 250°C, the interior tube surface shows intricate nanostructures (*a*,*b*). SEM micrograph areas: (*a*) $51 \times 33\,\mu m^2$, (*b*) $11 \times 7\,\mu m^2$. (*c*) High-resolution transmission electron microscopy image of tube fragments. Image area: $215 \times 150\,nm^2$. (*d*) Selected area electron diffraction patterns and corresponding Miller indices. (*e*) X-ray diffraction pattern of tube fragments. Reprinted with permission from Pagano *et al.* [60].

are washed, dried at room temperature and then heated to 200–250°C for 2 h. During this entire process, the samples maintain their tubular shape and approximate size. Materials characterization (including X-ray and electron diffraction; figure 9) of the resulting tubes reveals large concentrations of zinc oxide. While the conversion of zinc hydroxide to zinc oxide is not surprising at these temperatures, it is remarkable that the tubes neither collapse nor break. Moreover, one finds flake- or needle-like nanostructures on the interior surface of the heat-treated tubes. A representative image obtained by high-resolution SEM is shown in figure 9. In addition, the samples produced by this method show green photoluminescence under UV excitation (325 nm) and have photocatalytic activity. The latter characteristic was demonstrated for the photodegradation of an organic dye in aqueous solution [60].

8. Conclusions

In conclusion, we have described numerous aspects of silica tube growth, including distinct growth regimes, size selection and compositional as well as morphological features. Furthermore, we reviewed some of the experimental strategies put

forward in recent years that allow reproducible measurements and controlled perturbations. These advances provide the basis for theoretical work capable of describing quantitative details (e.g. radius and oscillation periods) with no or very few adjustable parameters.

Beyond this progress towards a satisfactory description of this class of reactions, many of the precipitation structures show interesting materials features such as photoluminescence and photocatalytic activity. Additional efforts are underway to expand this spectrum of materials characteristics. However, what makes these systems truly remarkable is their inherent architectural structure that extends from the molecular level all the way to macroscopic length scales in the range of several centimetres. This complexity is a direct consequence of the non-equilibrium conditions that give rise to the formation of the material. The combination of molecular, nanoscale and macroscopic characteristics could allow for interesting applications. A rather obvious example is the use of such tubes in microfluidic devices where they could serve as special processing segments or sensors. A simple proof of concept for this approach was published in Thouvenel-Romans & Steinbock [52]. Other applications could involve stacked tube arrays that would provide extremely low flow resistance to gas and liquids while exposing the fluids to large, chemically active surfaces.

Lastly, we note another remarkable feature that relates to the presence of steep concentration and pH gradients across the tube wall. During synthesis, these gradients occur naturally from the compartmentalization of the basic silicate and the acidic metal salt solution. However, these gradients can also be maintained after completion of the tube growth. Furthermore, it should be possible to create a multitude of different physical and chemical gradients simply by replacing the interior and exterior solutions. Whatever their nature and origin, these gradients will be steepest within the micrometre-sized tube wall, which in itself is a porous matrix that allows (slow) diffusion but prevents fluid flow [59,61,62]. These should be ideal conditions for carrying out numerous reactions, including convective polymerase chain reactions, Soret processes and possibly electrochemically driven energy production [63,64].

This work was supported by the National Science Foundation (grant no. 1005861). We thank Mohammed Al-Humiari and Stephanie Thouvenel-Romans for performing some of the experiments.

References

1 Mann, S. & Ozin, G. A. 1996 Synthesis of inorganic materials with complex form. *Nature* **382**, 313–318. (doi:10.1038/382313a0)

2 Grzybowski, B. A. 2009 *Chemistry in motion: reaction–diffusion systems for micro- and nanotechnology*. Chichester, UK: Wiley.

3 Mann, S. 2008 Life as a nanoscale phenomenon. *Angew. Chem. Int. Ed.* **47**, 5306–5320. (doi:10.1002/anie.200705538)

4 Loose, M., Fischer-Friedrich, E., Ries, J., Kruse, K. & Schwille, P. 2008 Spatial regulators for bacterial cell division self-organize into surface waves *in vitro*. *Science* **320**, 789–792. (doi:10.1126/science.1154413)

5 White, S. R., Sottos, N. R., Geubelle, P. H., Moore, J. S., Kessler, M. R., Sriram, S. R., Brown, E. N. & Viswanathan, S. 2001 Autonomic healing of polymer composites. *Nature* **409**, 794–797. (doi:10.1038/35057232)

6 Wool, R. P. 2008 Self-healing materials: a review. *Soft Matter* **4**, 400–418. (doi:10.1039/b711716g)

7 Wu, D. Y., Meure, S. & Solomon, D. 2008 Self-healing polymeric materials: a review of recent developments. *Prog. Polym. Sci.* **33**, 479–522. (doi:10.1016/j.progpolymsci.2008.02.001)
8 Makki, R., Al-Humiari, M., Dutta, S. & Steinbock, O. 2009 Hollow microtubes and shells from reactant-loaded polymer beads. *Angew. Chem. Int. Ed.* **48**, 8752–8756. (doi:10.1002/anie.200903292)
9 Maselko, J., Borisova, P., Carnahan, M., Dreyer, E., Devon, R., Schmoll, M. & Douthat, D. 2005 Spontaneous formation of chemical motors in simple inorganic systems. *J. Mater. Sci.* **40**, 4671–4673. (doi:10.1007/s10853-005-3926-z)
10 Paxton, W. F., Sundararajan, S., Mallouk, T. E. & Sen, A. 2006 Chemical locomotion. *Angew. Chem. Int. Ed.* **45**, 5420–5429. (doi:10.1002/anie.200600060)
11 Howse, J. R., Jones, R. A. L., Ryan, A. J., Gough, T., Vafabakhsh, R. & Golestanian, R. 2007 Self-motile colloidal particles: from directed propulsion to random walk. *Phys. Rev. Lett.* **99**, 048102. (doi:10.1103/PhysRevLett.99.048102)
12 Tao, Y.-G. & Kapral, R. 2008 Design of chemically propelled nanodimer motors. *J. Chem. Phys.* **128**, 164518. (doi:10.1063/1.2908078)
13 Corliss, J. B. *et al.* 1979 Submarine thermal springs on the Galápagos Rift. *Science* **203**, 1073–1083. (doi:10.1126/science.203.4385.1073)
14 Short, M. B., Baygents, J. C. & Goldstein, R. E. 2005 Stalactite growth as a free-boundary problem. *Phys. Fluids* **17**, 083101. (doi:10.1063/1.2006027)
15 Mann, S. 2001 *Biomineralization: principles and concepts in bioinorganic materials chemistry*. Oxford, UK: Oxford University Press.
16 Short, M., Baygents, J., Beck, J., Stone, D., Toomey, R. & Goldstein, R. 2005 Stalactite growth as a free-boundary problem: a geometric law and its platonic ideal. *Phys. Rev. Lett.* **94**, 018501. (doi:10.1103/PhysRevLett.94.018501)
17 Double, D. D., Hellawell, A. & Perry, S. J. 1978 The hydration of Portland cement. *Proc. R. Soc. Lond. A* **359**, 435–451. (doi:10.1098/rspa.1978.0050)
18 Stone, D. A., Lewellyn, B., Baygents, J. C. & Goldstein, R. E. 2005 Precipitative growth templated by a fluid jet. *Langmuir* **21**, 10 916–10 919. (doi:10.1021/la052064z)
19 Stone, D. A. & Goldstein, R. E. 2004 Tubular precipitation and redox gradients on a bubbling template. *Proc. Natl Acad. Sci. USA* **101**, 11 537–11 541. (doi:10.1073/pnas.0404544101)
20 Cartwright, J. H. E., Escribano, B., Khokhlov, S. & Sainz-Díaz, C. I. 2011 Chemical gardens from silicates and cations of group 2: a comparative study of composition, morphology and microstructure. *Phys. Chem. Chem. Phys.* **13**, 1030–1036. (doi:10.1039/c0cp01093f)
21 Cartwright, J. H. E., Escribano, B. & Sainz-Díaz, C. I. 2011 Chemical-garden formation, morphology, and composition. I. Effect of the nature of the cations. *Langmuir* **27**, 3286–3293. (doi:10.1021/la104192y)
22 Pagano, J. J., Bánsági, T. & Steinbock, O. 2007 Tube formation in reverse silica gardens. *J. Phys. Chem. C* **111**, 9324–9329. (doi:10.1021/jp071534q)
23 Bormashenko, E., Bormashenko, Y., Stanevsky, O. & Pogreb, R. 2006 Evolution of chemical gardens in aqueous solutions of polymers. *Chem. Phys. Lett.* **417**, 341–344. (doi:10.1016/j.cplett.2005.10.049)
24 Damerell, V. R. & Brock, H. 1949 Colloidal gardens from sodium metasilicate. *J. Chem. Educ.* **26**, 148. (doi:10.1021/ed026p148)
25 Roesky, H. & Möckel, K. 1996 *Chemical curiosities*. Weinheim, Germany: VCH.
26 Glauber, J. R. 1646 *Furni novi philiosophici*. Amsterdam, The Netherlands.
27 Leduc, S. 1911 *The mechanism of life*. London, UK: Rebman.
28 Mann, T. 1947 *Doktor faustus*. Stockholm, Sweden: Bermann-Fischer.
29 Sacks, O. 2001 *Uncle tungsten: memories of a chemical boyhood*. New York, NY: Vintage.
30 Keir, J. 1790 Experiments and observations on the dissolution of metals in acids, and their precipitations; with an account of a new compound acid menstruum, useful in some technical operations of parting metals. *Phil. Trans. R. Soc. Lond.* **80**, 359–384. (doi:10.1098/rstl.1790.0024)
31 Keir, J. 1776 On the crystallizations observed on glass. *Phil. Trans. R. Soc. Lond.* **66**, 530–542. (doi:10.1098/rstl.1776.0036)

32 Collins, C., Mann, G., Hoppe, E., Duggal, T., Barr, T. L. & Klinowski, J. 1999 NMR and ESCA studies of the 'silica garden' Brønsted acid catalyst. *Phys. Chem. Chem. Phys.* **1**, 3685–3687. (doi:10.1039/a904058g)

33 Collins, C., Mokaya, R. & Klinowski, J. 1999 The 'silica garden' as a Brønsted acid catalyst. *Phys. Chem. Chem. Phys.* **1**, 4669–4672. (doi:10.1039/a905296h)

34 Collins, C., Zhou, W., Mackay, A. L. & Klinowski, J. 1998 The 'silica garden': a hierarchical nanostructure. *Chem. Phys. Lett.* **286**, 88–92. (doi:10.1016/S0009-2614(98)00081-5)

35 Balköse, D., Özkan, F., Köktürk, U., Ulutan, S., Ülkü, S. & Nişli, G. 2002 Characterization of hollow chemical garden fibers from metal salts and water glass. *J. Sol-Gel Sci. Technol.* **23**, 253–263. (doi:10.1023/A:1013931116107)

36 Cartwright, J. H. E., García-Ruiz, J. M., Novella, M. L. & Otálora, F. 2002 Formation of chemical gardens. *J. Colloid Interface Sci.* **256**, 351–359. (doi:10.1006/jcis.2002.8620)

37 Jones, D. E. H. & Walter, U. 1998 The silicate garden reaction in microgravity: a fluid interfacial instability. *J. Colloid Interface Sci.* **203**, 286–293. (doi:10.1006/jcis.1998.5447)

38 Jones, D. 2002 Gardening in space. *Am. Sci.* **90**, 454–461. (doi:10.1511/2002.5.454)

39 Cartwright, J. H. E., Escribano, B., Sainz-Diìaz, C. I. & Stodieck, L. S. 2011 Chemical-garden formation, morphology, and composition. II. Chemical gardens in microgravity. *Langmuir* **27**, 3294–3300. (doi:10.1021/la104193q)

40 Ritchie, C., Cooper, G. J. T., Song, Y.-F., Streb, C., Yin, H., Parenty, A. D. C., MacLaren, D. A. & Cronin, L. 2009 Spontaneous assembly and real-time growth of micrometre-scale tubular structures from polyoxometalate-based inorganic solids. *Nat. Chem.* **1**, 47–52. (doi:10.1038/nchem.113)

41 Cooper, G. J. T. *et al.* 2011 Osmotically driven crystal morphogenesis: a general approach to the fabrication of micrometer-scale tubular architectures based on polyoxometalates. *J. Am. Chem. Soc.* **133**, 5947–5954. (doi:10.1021/ja111011j)

42 Cooper, G. J. T. & Cronin, L. 2009 Real-time direction control of self fabricating polyoxometalate-based microtubes. *J. Am. Chem. Soc.* **131**, 8368–8369. (doi:10.1021/ja902684b)

43 Pantaleone, J. *et al.* 2008 Oscillations of a chemical garden. *Phys. Rev. E* **77**, 046207. (doi:10.1103/PhysRevE.77.046207)

44 Pantaleone, J., Tóth, Á., Horváth, D., RoseFigura, L., Morgan, W. & Maselko, J. 2009 Pressure oscillations in a chemical garden. *Phys. Rev. E* **79**, 056221. (doi:10.1103/PhysRevE.79.056221)

45 Russell, M. J., Hall, A. J., Cairns-Smith, A. G. & Braterman, P. S. 1988 Submarine hot springs and the origin of life. *Nature* **336**, 117. (doi:10.1038/336117a0)

46 Russell, M. J. & Hall, A. J. 1997 The emergence of life from iron monosulphide bubbles at a submarine hydrothermal redox and pH front. *J. Geol. Soc. Lond.* **154**, 377–402. (doi:10.1144/gsjgs.154.3.0377)

47 Vairavapandian, D., Vichchulada, P. & Lay, M. D. 2008 Preparation and modification of carbon nanotubes: review of recent advances and applications in catalysis and sensing. *Anal. Chim. Acta* **626**, 119–129. (doi:10.1016/j.aca.2008.07.052)

48 Nakamura, H. & Matsui, Y. 1995 Silica gel nanotubes obtained by the sol–gel method. *J. Am. Chem. Soc.* **117**, 2651–2652. (doi:10.1021/ja00114a031)

49 Nakamura, H. & Matsui, Y. 1995 The preparation of novel silica gel hollow tubes. *Adv. Mater.* **7**, 871–872. (doi:10.1002/adma.19950071013)

50 Chaudhary, Y. S., Ghatak, J., Bhatta, U. M. & Khushalani, D. 2006 One-step method for the self-assembly of metal nanoparticles onto facetted hollow silica tubes. *J. Mater. Chem.* **16**, 3619–3623. (doi:10.1039/b608460e)

51 Miyaji, F., Davis, S. A., Charmant, J. P. H. & Mann, S. 1999 Organic crystal templating of hollow silica fibers. *Chem. Mater.* **11**, 3021–3024. (doi:10.1021/cm990449v)

52 Thouvenel-Romans, S. & Steinbock, O. 2003 Oscillatory growth of silica tubes in chemical gardens. *J. Am. Chem. Soc.* **125**, 4338–4341. (doi:10.1021/ja0298343)

53 Thouvenel-Romans, S., Saarloos, W. & Steinbock, O. 2004 Silica tubes in chemical gardens: radius selection and its hydrodynamic origin. *Europhys. Lett.* **67**, 42–48. (doi:10.1209/epl/i2003-10279-7)

54 Hazlehurst, T. H. 1941 Structural precipitates: the silicate garden type. *J. Chem. Educ.* **18**, 286–289. (doi:10.1021/ed018p286)

55 Thouvenel-Romans, S., Pagano, J. J. & Steinbock, O. 2005 Bubble guidance of tubular growth in reaction–precipitation systems. *Phys. Chem. Chem. Phys.* **7**, 2610–2615. (doi:10.1039/B504407C)
56 Makki, R. & Steinbock, O. 2011 Synthesis of inorganic tubes under actively controlled growth velocities and injection rates. *J. Phys. Chem. C* **115**, 17 046–17 053. (doi:10.1021/jp2046849)
57 Müller, I. & Strehlow, P. 1999 Physik von luftballons. *Physik. Blätter* **55**, 37–41.
58 Pagano, J. J., Thouvenel-Romans, S. & Steinbock, O. 2007 Compositional analysis of copper–silica precipitation tubes. *Phys. Chem. Chem. Phys.* **9**, 110–116. (doi:10.1039/B612982J)
59 Roszol, L. & Steinbock, O. 2011 Controlling the wall thickness and composition of hollow precipitation tubes. *Phys. Chem. Chem. Phys.* **13**, 20 100–20 113. (doi:10.1039/C1CP22556A)
60 Pagano, J. J., Bánsági, T. & Steinbock, O. 2008 Bubble-templated and flow-controlled synthesis of macroscopic silica tubes supporting zinc oxide nanostructures. *Angew. Chem. Int. Ed.* **47**, 9900–9903. (doi:10.1002/anie.200803203)
61 Ayalon, A. 1984 Precipitation membranes: a review. *J. Membr. Sci.* **20**, 93–102. (doi:10.1016/S0376-7388(00)80725-5)
62 Bähr, G., Ayalon, A., Rompf, F. D. & Hirsch-Ayalon, P. 1984 Discrimination between the permeation of H^+ and OH^- ions in precipitation membranes. *J. Membr. Sci.* **20**, 103–111. (doi:10.1016/S0376-7388(00)80726-7)
63 Mast, C. B. & Braun, D. 2010 Thermal trap for DNA replication. *Phys. Rev. Lett.* **104**, 188102. (doi:10.1103/PhysRevLett.104.188102)
64 Maeda, Y. T., Buguin, A. & Libchaber, A. 2011 Thermal separation: interplay between the Soret effect and entropic force gradient. *Phys. Rev. Lett.* **107**, 038301. (doi:10.1103/PhysRevLett.107.038301)